■ 5.16 AXIAL FLOW COMPRESSOR

A schematic diagram of an axial flow compressor is shown in Fig. 5.28. It consists of a number of fixed blades attached to the casing and alternate rows of moving blades are fixed on a central drum, which rotates along with the shaft. Air progresses from one blade row to the next and is guided by the fixed blades. Fixed blades serve the function of a diffuser and hence the pressure of air increases when it comes out of the duct. As air passes parallel to the axis of rotation of the shaft, the flow is axial and hence the name axial flow compressor. These compressors usually run at high speed (10,000 – 30,000 rpm) and are employed to supply large quantity of air as in aircraft gas turbines. The pressure ratio of compression may be about 10 : 1.

Due to rapid compression time available for heat transfer is less and hence compression is nearly adiabatic. However, due to generation of friction and turbulence, internal energy within air generates temperature which is higher than the adiabatic temperature. Thus the index 'n' is greater than adiabatic index 'γ' for a rotary compressor.

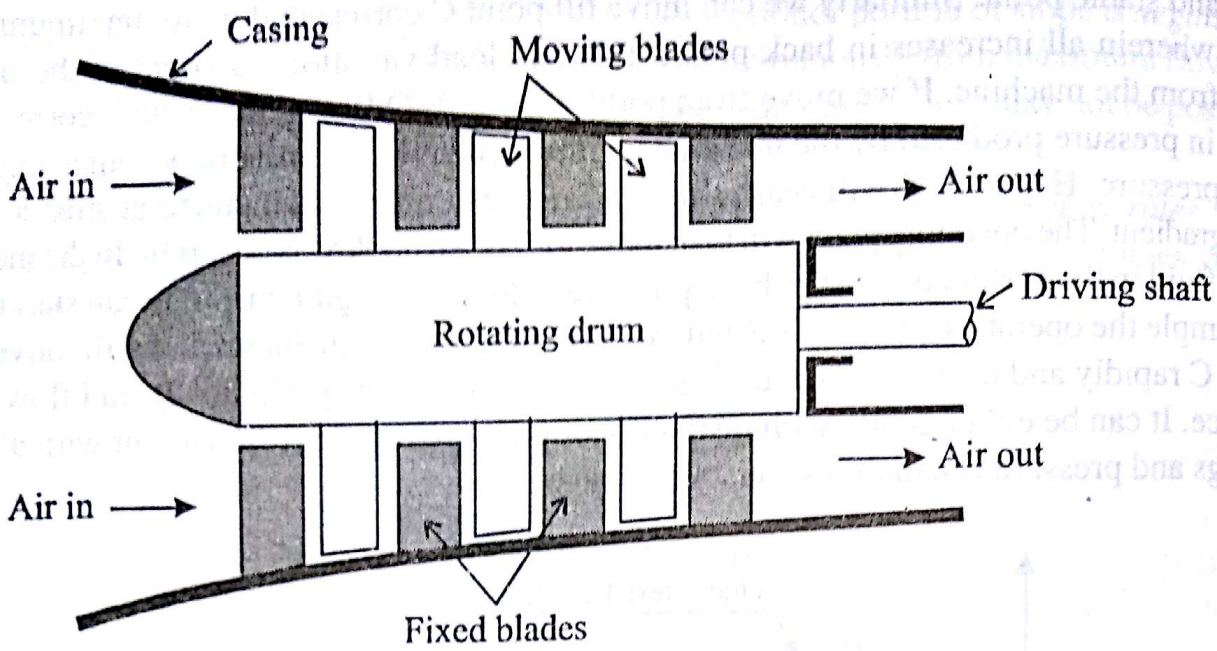

Fig. 5.28 : Axial flow compressor with drum type rotor

As shown in the figure 5.28, the compressor consists of alternate sets of moving and fixed blades. The sets of fixed blades which are spaced around an outer stationary casing are called **stator blades**, and the sets of moving blades fixed to a spindle are called **rotor blades.** A very small tip clearance at the end of the stator and rotor blades are provided to ensure smooth and efficient flow. A compressor stage consists of one set of stator blades and one set of rotor blades. Depending on the pressure ratio required, stage may be either single or multiple. In multistage arrangement the successive sets of blades are reduced in length to compensate for reduction in volume resulting due to pressure increase from stage to stage.

An axial compressor may have either disc type rotor or drum type rotor. For the same overall weight centrifugal stresses are lower in the disc type than in the drum type.

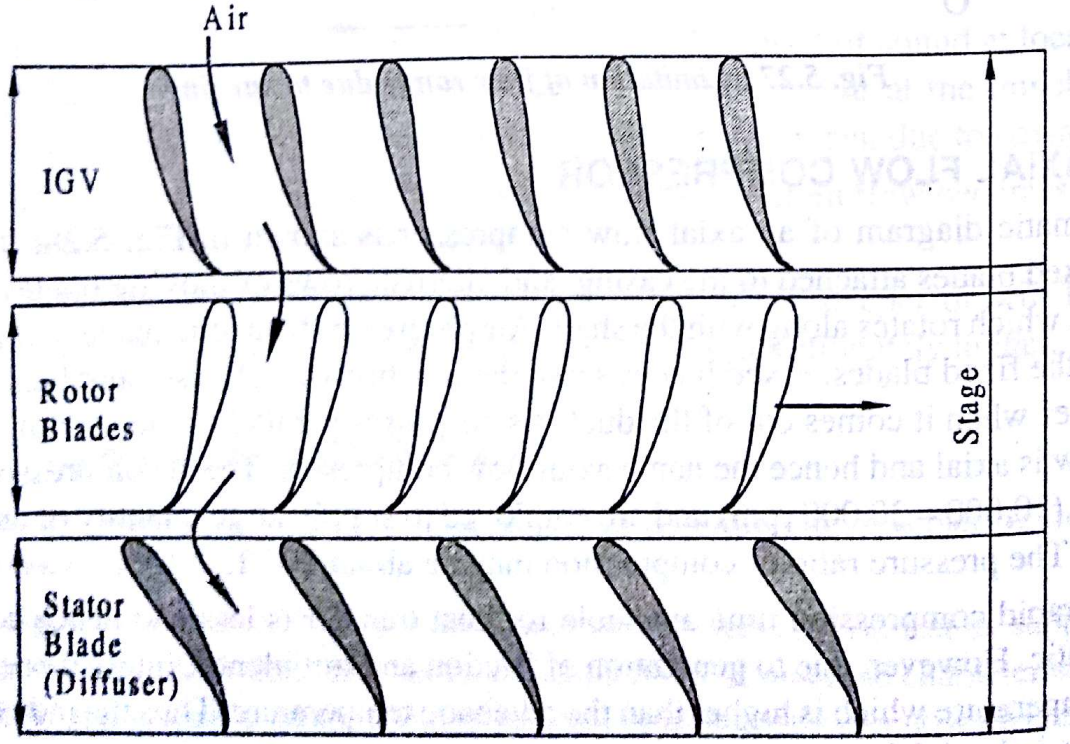

Fig. 5.29 : An axial compressor stage

The basic principle of operation of an axial flow compressor is similar to that of a centrifugal type. Here, the rotating blades impart kinetic energy to air which is further converted into pressure rise. Stator recovers part of kinetic energy imparted to the working fluid and redirects the fluid to the rotating blades of next stage at a convenient angle. Air is guided to the rotor blades using *IGV*'s (inlet guide vanes) as shown in figure 5.29. Air enters the combustion chamber through one to three rows of diffuser blades or straightener blades installed after the last stage. This is to ensure that air is straightened and skewed down before it enters the combustion chamber.

■ 5.17 STAGE VELOCITY TRIANGLES

Figure 5.30 shows the velocity triangles for an axial compressor stage. Subscripts 1, 2, 3 correspond to condition of air at entry to rotor, exit from rotor and diffuser blades respectively.

Let α_1, α_2, α_3 and β_1, β_2 be the air angles in the absolute and relative systems respectively. Subscripts *a*, *u* represent axial, tangential component of absolute velocity respectively and *ru* represents tangential component of relative velocity *Vr*.

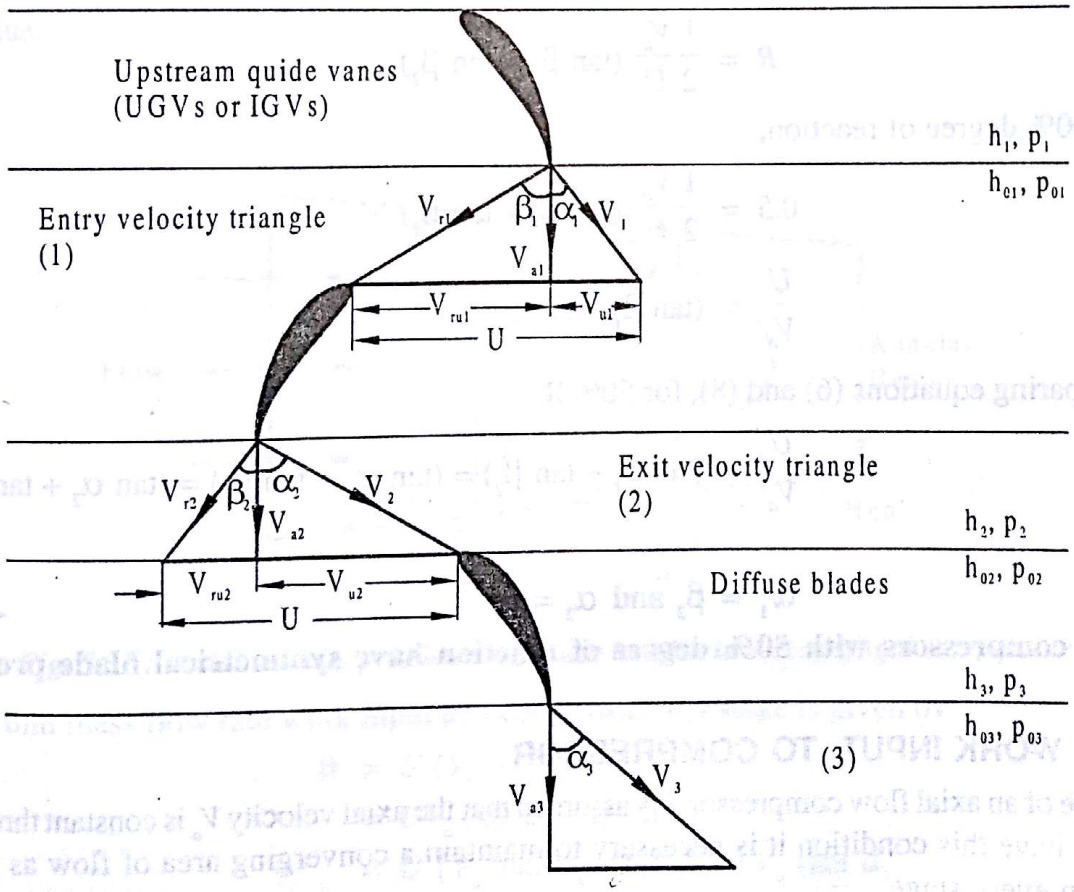

Fig. 5.30 : Velocity triangles for a compressor stage

From the entry velocity triangle,

$$U = V_{u1} + V_{ru_1}$$

$$U = V_1 \sin \alpha_1 + V_{r1} \sin \beta_1 \quad \text{----- (1)}$$

$$U = V_{a1} (\tan \alpha_1 + \tan \beta_1) \quad \text{----- (2)}$$

From the exit velocity triangle,

$$U = V_{u2} + V_{ru2}$$

$$U = V_2 \sin \alpha_2 + V_{r2} \sin \beta_2 \quad \text{----- (3)}$$

$$U = V_{a2} (\tan \alpha_2 + \tan \beta_2) \quad \text{----- (4)}$$

If axial velocity is constant through the stage

$$V_{a1} = V_{a2} = V_{a3} = V_a$$

$$V_a = V_1 \cos \alpha_1 = V_{r1} \cos \beta_1 = V_2 \cos \alpha_2 = V_{r2} \cos \beta_2 \quad \text{----- (5)}$$

From equations (2) and (4),

$$\frac{U}{V_a} = \frac{1}{\phi} = \tan \alpha_1 + \tan \beta_1 = \tan \alpha_2 + \tan \beta_2 \quad \text{----- (6)}$$

Rearranging the above relation

$$(\tan \alpha_2 - \tan \alpha_1) = (\tan \beta_1 - \tan \beta_2) \quad \text{----- (7)}$$

Now, degree of reaction is given by

$$R = \frac{1}{2} \frac{V_a}{U} (\tan \beta_1 + \tan \beta_2)$$

For 50% degree of reaction,

$$0.5 = \frac{1}{2} \frac{V_a}{U} (\tan \beta_1 + \tan \beta_2)$$

or

$$\frac{U}{V_a} = (\tan \beta_1 + \tan \beta_2) \quad \text{----- (8)}$$

Comparing equations (6) and (8), for 50% R

$$\frac{U}{V_a} = (\tan \beta_1 + \tan \beta_2) = (\tan \alpha_1 + \tan \beta_1) = (\tan \alpha_2 + \tan \beta_2) \text{ ---- (9)}$$

or

$$\alpha_1 = \beta_2 \text{ and } \alpha_2 = \beta_1 \quad \text{----- (10)}$$

Thus **compressors with 50% degree of reaction have symmetrical blade profile.**

■ 5.18 WORK INPUT TO COMPRESSOR

In case of an axial flow compressor it is assumed that the axial velocity V_a is constant throughout. In order to have this condition it is necessary to maintain a converging area of flow as pressure increases in every stage.

From equation (6)

$$U = V_a (\tan \alpha_1 + \tan \beta_1) = V_a (\tan \alpha_2 + \tan \beta_2)$$

and work input

$$W = U (V_{u2} - V_{u1})$$

$$= U (V_a \tan \alpha_2 - V_a \tan \alpha_1)$$

$$W = UV_a (\tan \alpha_2 - \tan \alpha_1) \quad \text{----- (1)}$$

$$W = UV_a (\tan \beta_1 - \tan \beta_2) \quad \text{----- (2)}$$

From Euler's equation,

$$E = \frac{1}{2}(V_2^2 - V_1^2) + \frac{1}{2}(V_{r1}^2 - V_{r2}^2) \quad \text{----- (3)}$$

as U = constant throughout.

■ 5.19 WORK DONE FACTOR

Figure 5.31 shows the axial velocity distributions along the blade heights in the first and last rows of blades of a multistage compressor. It can be noted that due to secondary flows and growth of the boundary layers on the hub and the casing of the compressor annulus, the axial velocity is not uniform. In a multistage compressor this effect is considerable after the first stage and the degree of distortion depends on the number of stages. Owing to this effect the axial velocity in the hub and tip regions is much lesser than the mean value whereas in the central zone it is much higher than mean value.

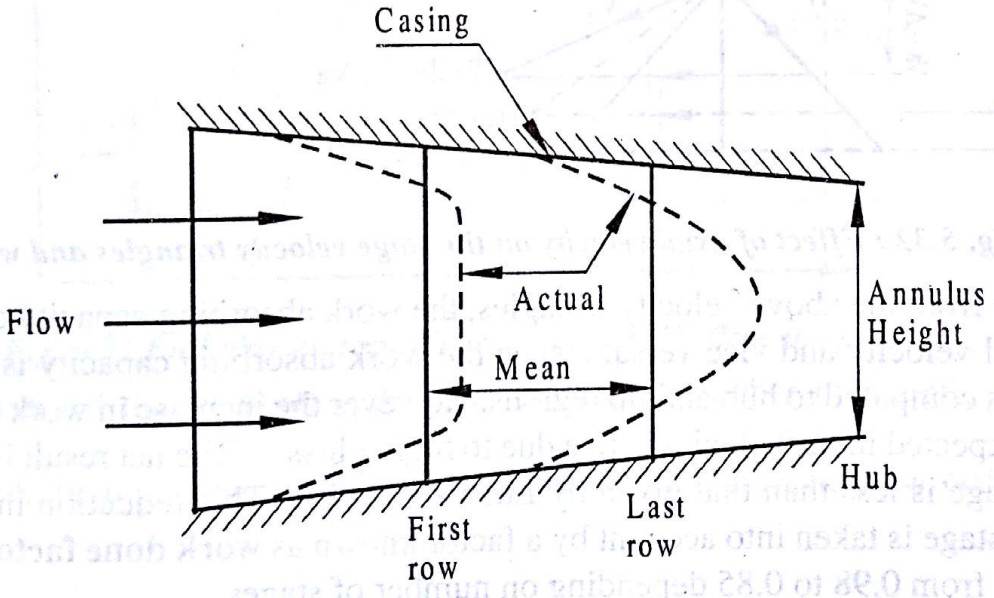

Fig. 5.31 : Axial velocity profile along blade heights in a centrifugal compressor

For unit mass flow rate work input to a compressor per stage is given by

$$W = U(V_{u2} - V_{u1})$$
$$= UV_a (\tan \beta_1 - \tan \beta_2)$$
$$= U\{V_a (\tan \alpha_1 + \tan \beta_1) - V_a (\tan \alpha_1 + \tan \beta_2)\} \quad \text{----- (1)}$$

Substituting from equation (6) of ■5.17, in (1)

$$\frac{U}{V_a} = \tan \alpha_1 + \tan \beta_1 = \tan \alpha_2 + \tan \beta_2 = \frac{1}{\phi} \quad \text{----- (2)}$$

$$\therefore \quad W = U\{U - V_a (\tan \alpha_1 + \tan \beta_2)\} \quad \text{----- (3)}$$

In the above relation air angles β_2 and α_1 are fixed by the cascade geometry of the rotor blades and the upstream blade row. Thus the above relation relates work to axial velocity at various sections along the blade height.

Figure 5.32 shows the effect of axial velocity on the stage velocity triangles and work. The velocity triangles thus drawn refer to mean value or design value, reduced value $(V_a - \Delta V_a)$ and increased value $(V_a + \Delta V_a)$ of axial velocity.

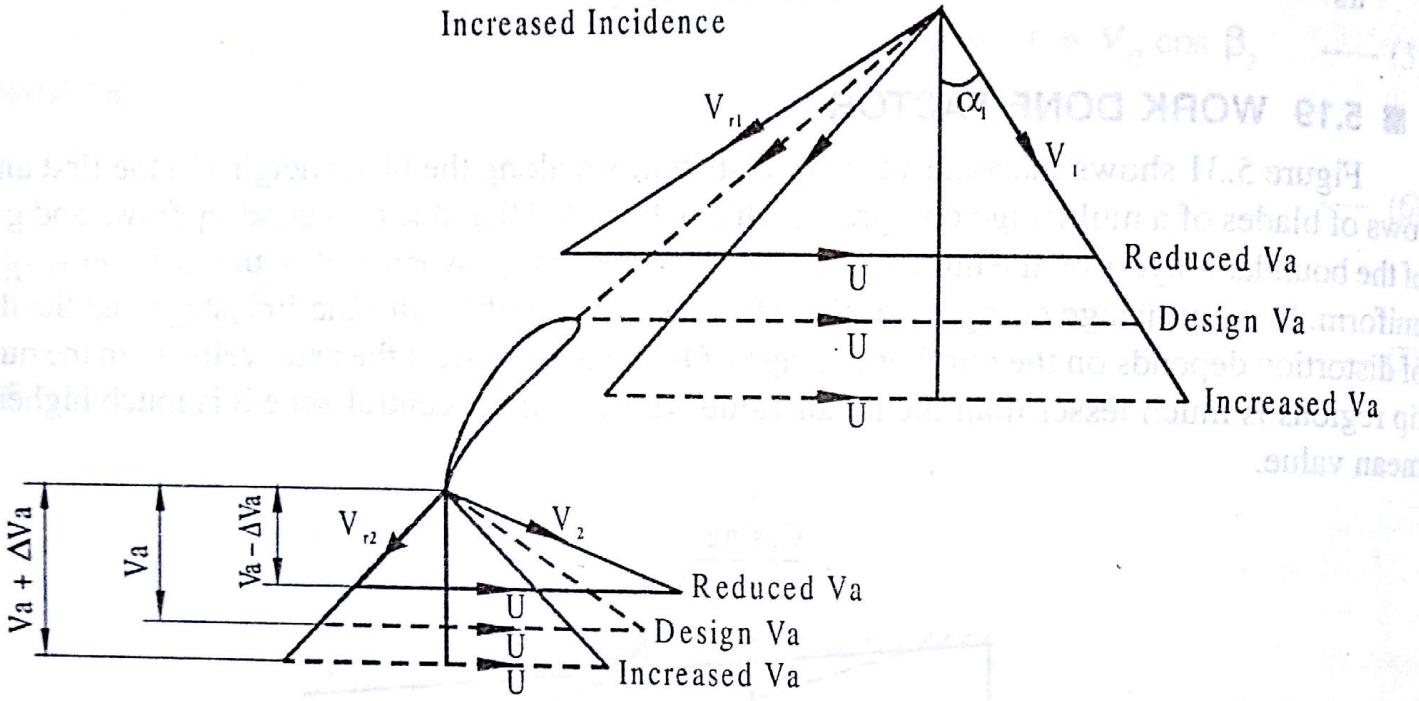

Fig. 5.32 : Effect of axial velocity on the stage velocity triangles and work

As evident from the above velocity triangles, the work absorbing capacity decreases with an increase in axial velocity and vice versa. Hence the work absorbing capacity is decreased in the central region as compared to hub and tip regions. However the increase in work at the hub and tip regions is not expected in the actual practice due to higher losses. The net result is work absorbing capacity in a stage is less than that given by Euler's equation. This reduction in work absorbing capacity of the stage is taken into account by a factor known as **work done factor**, denoted by Ω. Its value ranges from 0.98 to 0.85 depending on number of stages.

Considering work done factor, work done on air is given by,

$$W = \Omega\, UV_a (\tan \beta_1 - \tan \beta_2) \quad \text{----- (4)}$$

Since, $W = C_P \Delta T_s = C_P (To_2 - To_1)$, we have

$$\Delta T_s = \frac{\Omega U V_a}{C_P} (\tan \beta_1 - \tan \beta_2) \quad \text{----- (5)}$$

Where, ΔT_s is the stagnation temperature rise in stage.

Work done factor thus is a measure of the ratio of actual work absorbing capacity of the stage to its ideal value.

■ 5.20 COMPRESSOR STAGE EFFICIENCY

Figure 5.33 shows the enthalpy-entropy diagram for a general axial flow compressor stage. State points with superscript, correspond to isentropic compression processes. Air enters the rotor blades with lower absolute velocity, V_1 and leaves with large V_2. This velocity is reduced to V_3 when it passes through the diffuser blades which is slightly higher than V_1.

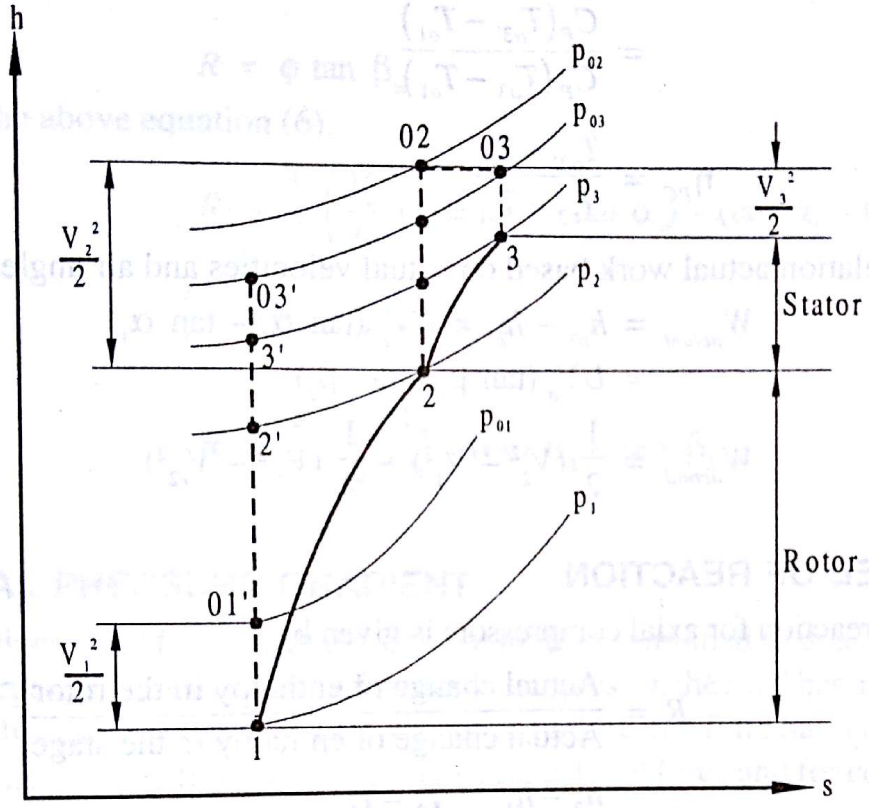

Fig. 5.33 Enthalpy-entropy diagram of an axial flow compressor.

It can be observed that stagnation pressure p_{o1} will be higher than static pressure by an amount $\frac{V_1^2}{2}$. Similarly p_{o2} is much higher than static pressure p_2. The flow occurs at constant enthalpy. Thus,

$$h_{o2} = h_{o3}$$

$$h_2 + \frac{V_2^2}{2} = h_3 + \frac{V_3^2}{2} \qquad \text{----- (1)}$$

Actual energy transformation in the rotor (1 – 2) and diffuser (2 – 3) occur with stagnation pressure loss and increase in entropy. However the relative stagnation enthalpy based on relative velocity remains constant.

$$h_{o1\,rel} = h_{o2\,rel}$$

$$h_1 + \frac{V_{r1}^2}{2} = h_2 + \frac{V_{r2}^2}{2} \qquad \text{----- (2)}$$

The stage efficiency of the compressor based on stagnation conditions at entry and exit is given by,

$$\eta_{pc} = \frac{W_{ideal}}{W_{actual}}$$

$$= \frac{h_{o3'} - h_{o1}}{h_{o3} - h_{o1}}$$

$$= \frac{C_P(T_{o3'} - T_{o1})}{C_P(T_{o3} - T_{o1})}$$

$$\eta_{PC} = \frac{T_{o3'} - T_{o1}}{T_{o3} - T_{o1}} \quad \text{----- (3)}$$

In the above relation actual work based on actual velocities and air angles may be given by,

$$W_{actual} = h_{o3} - h_{o1} = UV_a (\tan \alpha_2 - \tan \alpha_1)$$

$$= UV_a (\tan \beta_1 - \tan \beta_2)$$

$$W_{actual} = \frac{1}{2}(V_2^2 - V_1^2) + \frac{1}{2}(V_{r1}^2 - V_{r2}^2) \quad \text{----- (4)}$$

9.5 ENTHALPY–ENTROPY DIAGRAM

Figure 9.6 shows the enthalpy–entropy diagram for a general axial flow compressor stage. Static and stagnation values of pressures and enthalpies at various stations are as shown in Fig.9.6. 1–2′–3′ shows isentropic compression whereas 1–2–3 shows actual compression. The stagnation point 03′ corresponds to the final state at the end of isentropic compression.

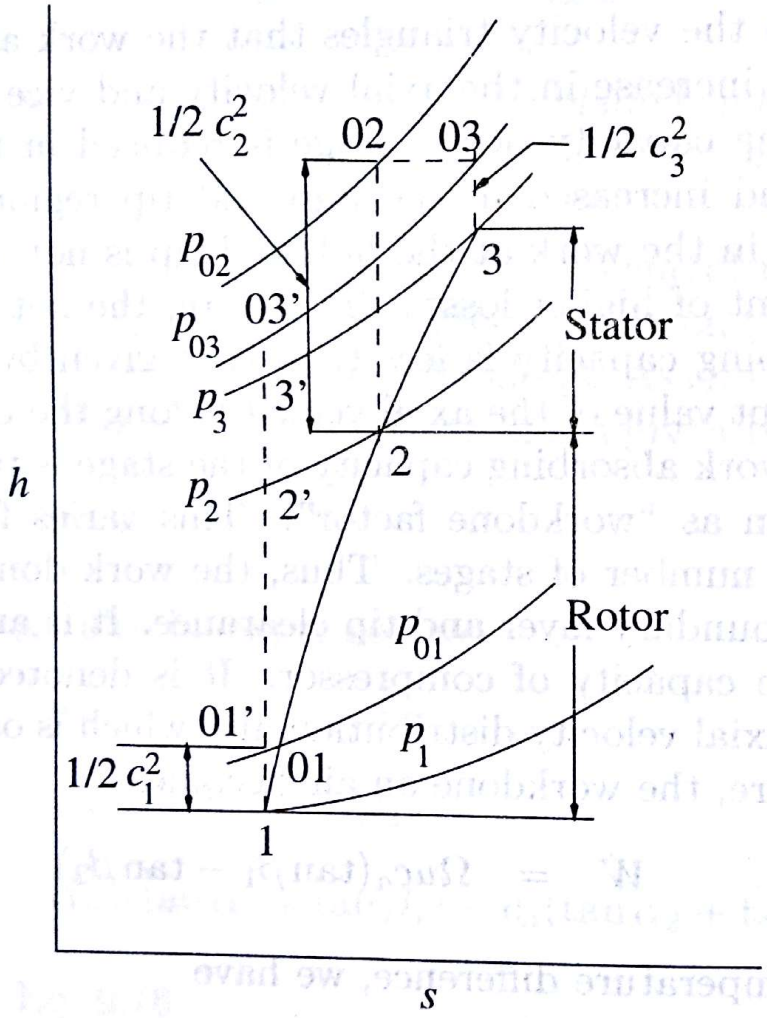

Fig. 9.6 Enthalpy–entropy diagram of an axial compressor

From Fig.9.3 it can be seen that air enters the rotor blades with lower absolute velocity (c_1) but with large relative velocity (w_1) whereas it leaves the rotor with large c_2 and lower w_2. However, when it comes out of the

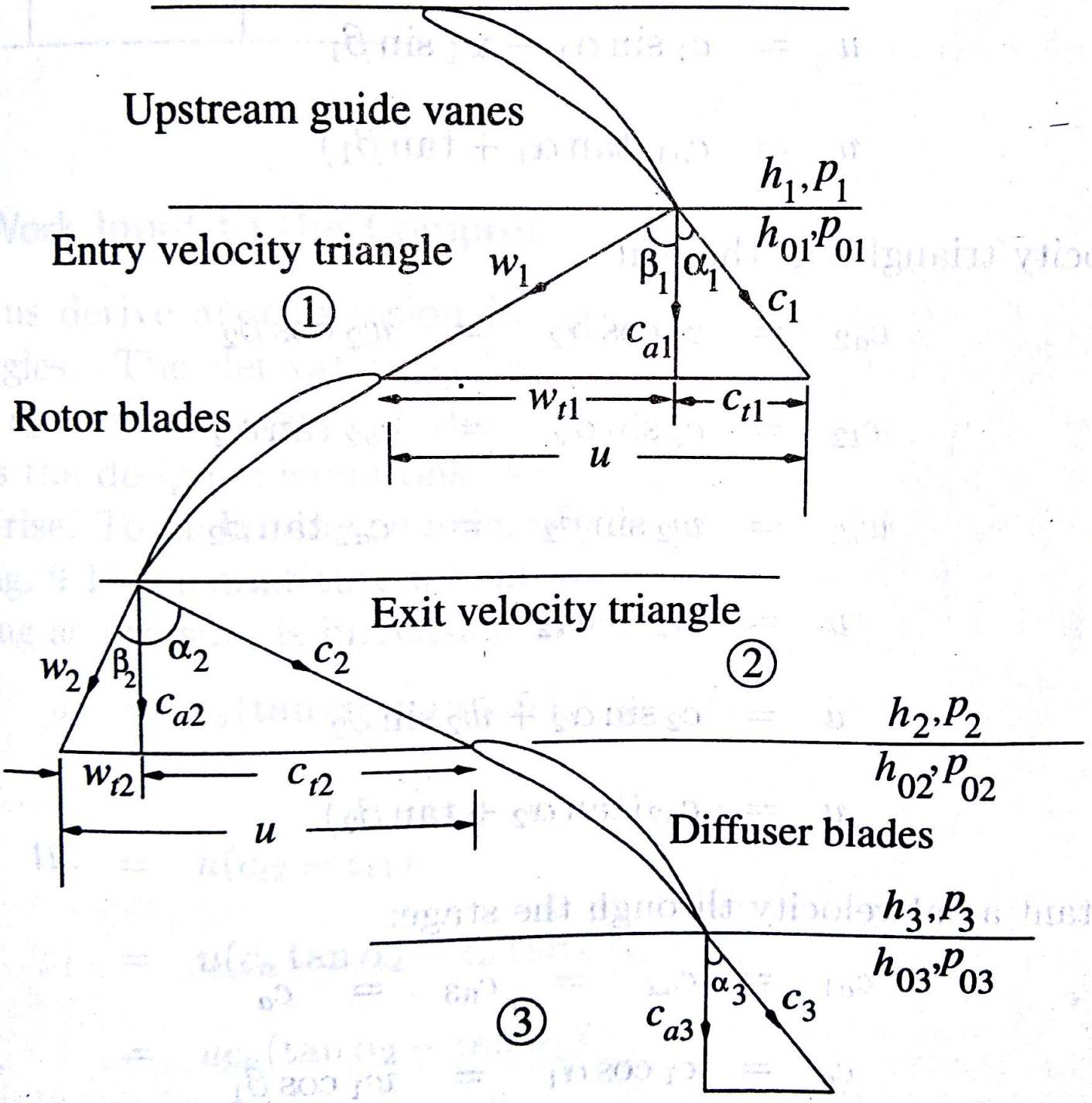

Fig. 9.3 Velocity triangles for a compressor stage

diffuser blades c_3 is reduced which will be close to (very slightly higher) c_1. Hence the stagnation pressure p_{01} will be slightly higher than the static pressure p_1 by $\frac{1}{2}c_1^2$ which is shown in Fig.9.6. However, the stagnation pressure p_{02} will be much higher than the static pressure p_2 as can be seen from the Fig.9.6. However, the flow occurs at constant enthalpy as can been seen in the figure. That is

$$\begin{aligned} h_{02} &= h_{03} \\ h_2 + \frac{1}{2}c_2^2 &= h_3 + \frac{1}{2}c_3^2 \end{aligned} \tag{9.32}$$

Further, it should be noted that the actual energy transformation process $(1-2)$ and $(2-3)$ in the rotor and diffuser blade rows occur with stagnation pressure loss and increase in entropy. However, the relative stagnation enthalpy remains constant.

$$\begin{aligned} h_{01\ rel} &= h_{02\ rel} \\ h_1 + \frac{1}{2}w_1^2 &= h_2 + \frac{1}{2}w_2^2 \end{aligned} \tag{9.33}$$

9.10 FLOW LOSSES

Principal aerodynamic losses occurring in most of the turbomachines arise due to the growth of the boundary layer and its separation on the blade and passage surfaces. Others occur due to wasteful circulatory flows and the formation of shock waves. Non-uniform velocity profiles at the exit of the

cascade lead to another type of loss referred to as the mixing or equalization loss.

Aerodynamic losses occurring in a turbomachine blade cascade can be grouped in the following categories.

9.10.1 Profile Loss

As the term indicates, this loss is associated with the growth of the boundary layer on the blade profile. Separation of the boundary layer occurs when the adverse pressure gradient on the surface or surfaces becomes too steep; this increases the profile loss. The pattern of the boundary layer growth and its separation depend on the geometries of the blade and the flow. Positive and negative stall losses occur on account of increased positive or negative incidences respectively.

Generally, the suction surface of a blade is more prone to boundary layer separation. The separation point depends besides the blade profile on factors like the degree of turbulence, Reynolds number and the incidence.

If the flow is initially supersonic or becomes supersonic on the blade surface additional losses occur due to the formation of shock waves resulting from the local deceleration of supersonic flow to subsonic.

9.10.2 Annulus Loss

The majority of blade rows in turbomachines are housed in casings. The axial compressor stage has a pair of fixed and moving blade rows.

In stationary blade rows a loss of energy occurs due to the growth of the boundary layer on the end walls. This also occurs in the rotating row of blades but the flow on the end walls in this case is subjected to effects associated with the rotation of the cascade. The boundary layer on the floor (hub) of the blade passages is subjected to centrifugal force, whereas that on the ceiling (outer casing) is scrapped by the moving blades.

9.10.3 Secondary Loss

This loss occurs in the regions of flow near the end walls owing to the presence of unwanted circulatory or cross flows. Such secondary flows develop on account of turning of the flow through the blade channel in the presence of annulus wall boundary layers. Figure 9.13 depicts the pressure gradients across a blade channel and the secondary and trailing vortices. Static pressure gradients from the suction to the pressure side in the regions away from the hub and tip are represented by the curve AB. In the vicinity of the hub and tip or the end walls the pressure gradient curve CD is not so steep on account of much lower velocities due to the wall boundary layers. Thus the static pressures at the four corners of the section of flow under considerations are

$$p_B > p_D > p_C > p_A$$

These pressure differentials across the flow near the end walls give rise

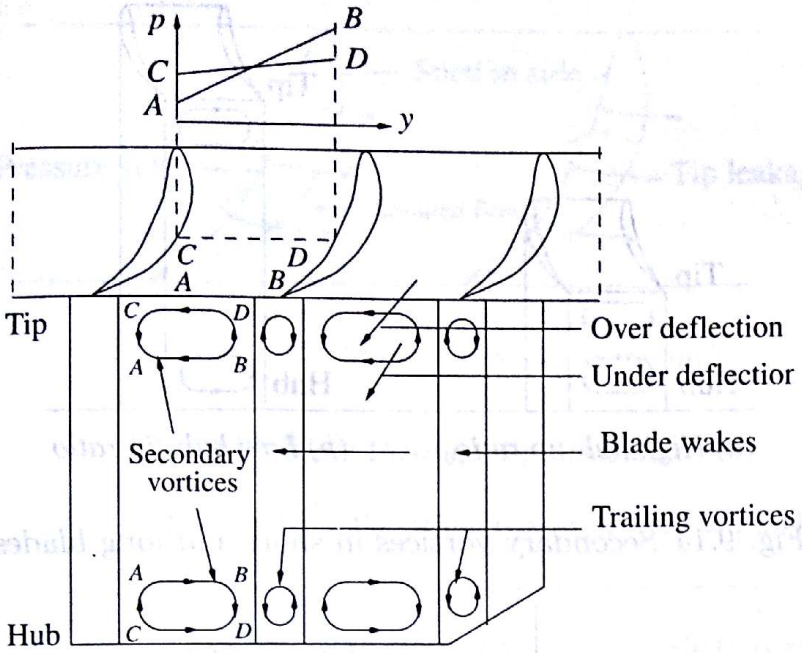

Fig. 9.13 Secondary flow in a cascade of blades

to circulatory flows which are superimposed on the main flow through the blade passage. As a result of this, secondary vortices in the streamwise direction are generated in the blade passages. These vortices, besides wasteful expenditure of fluid's energy, transport (DC) low energy fluid from the pressure to the suction side of the blade passage, thus increasing the possibility of an early separation of the boundary layer on the suction side. The flow nearer the hub and tip is over-deflected while that slightly away from the end walls is under-deflected as shown in Fig.9.13.

The secondary vortices in the adjacent blade channels induce vortices in the wake regions (as shown in Fig.9.13). These trailing vortices lead to additional losses. It is worth observing here that the secondary flows in the cascade also affect the profile and annulus losses.

The magnitude of the loss due to secondary flow depend on the fraction of the passage height that is affected by this flow. Blade passages of very low height (aspect ratio) or high hub-tip ratio are likely to be fully occupied by secondary vortices as shown in Fig.9.14(a), and experience higher secondary losses. In contrast to this longer blades [Fig.9.14(b)] have a large proportion of the flow free of secondary flows and therefore experience comparatively lower secondary losses.

If the total losses in a blade passage are measured along its height, they appear as peaks near the hub and tip on account of secondary losses. The flow in the central region which is outside the influence of secondary flows (particularly in longer blades) can be assumed to suffer only profile loss. Figure 9.15 illustrates this pattern of losses along the blade height.

9.10.4 Tip Clearance Loss

This loss arises due to the clearance between a moving blade and the casing. In a turbine rotor blade ring the suction sides lead and the pressure sides

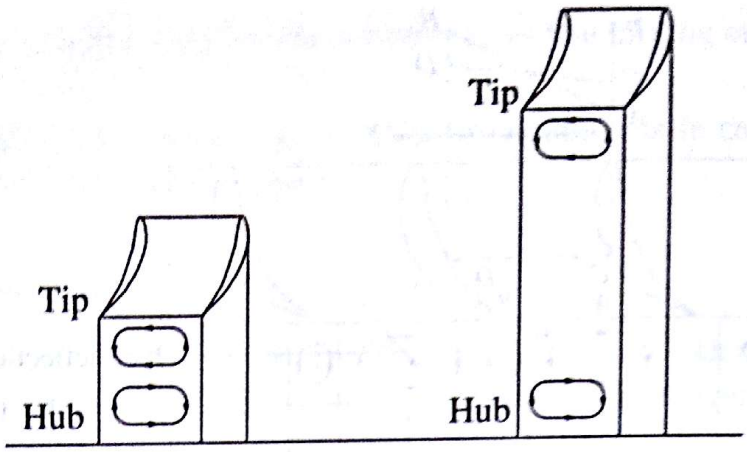

Fig. 9.14 Secondary vortices in short and long blades

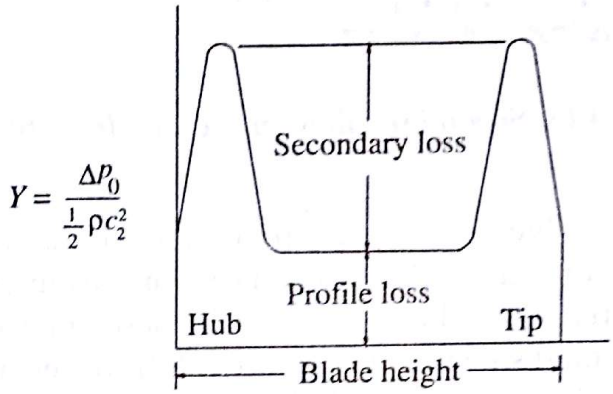

Fig. 9.15 Variation of losses along the blade height

trail. On account of the static pressure difference, the flow leaks from the pressure side towards the suction side as shown in Fig.9.16. However, due to the scrapping up of the casing boundary layer by the blade tips, the scrapped up flow opposes the aforementioned tip leakage. The tip clearance and secondary flows are closely related to each other and it is often convenient to estimate them together.

9.11 STAGE LOSSES

Figure 9.17 shows the energy flow diagram for an axial flow compressor stage. Figures in the brackets indicate the order of energy or loss corresponding to 100 units of energy supplied at the shaft.

The stage work $(h_{03} - h_{01})$ is less than the energy supplied to the shaft by the prime mover on account of bearing and disc friction losses. All the stage work does not appear as energy at the stator entry on account of aerodynamic losses in the rotor blade row. After deducting the stator (diffuser) blade row losses from the energy at its entry, the value of the ideal or isentropic work required to obtain the stage pressure rise is obtained.

The cascade losses in the rotor and stator would depend on the degree of reaction. The values shown in the energy flow diagram are only to give

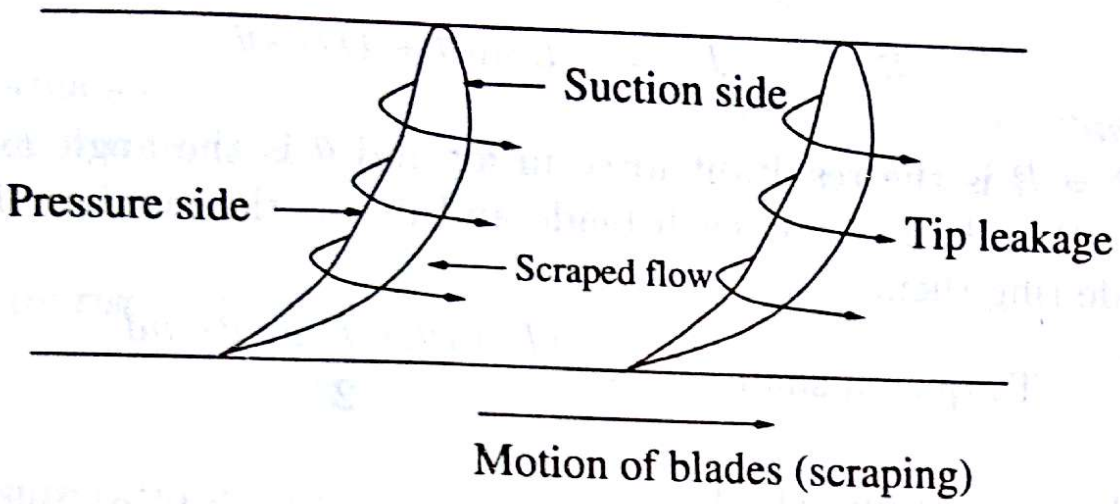

Fig. 9.16 Flow through tip clearance

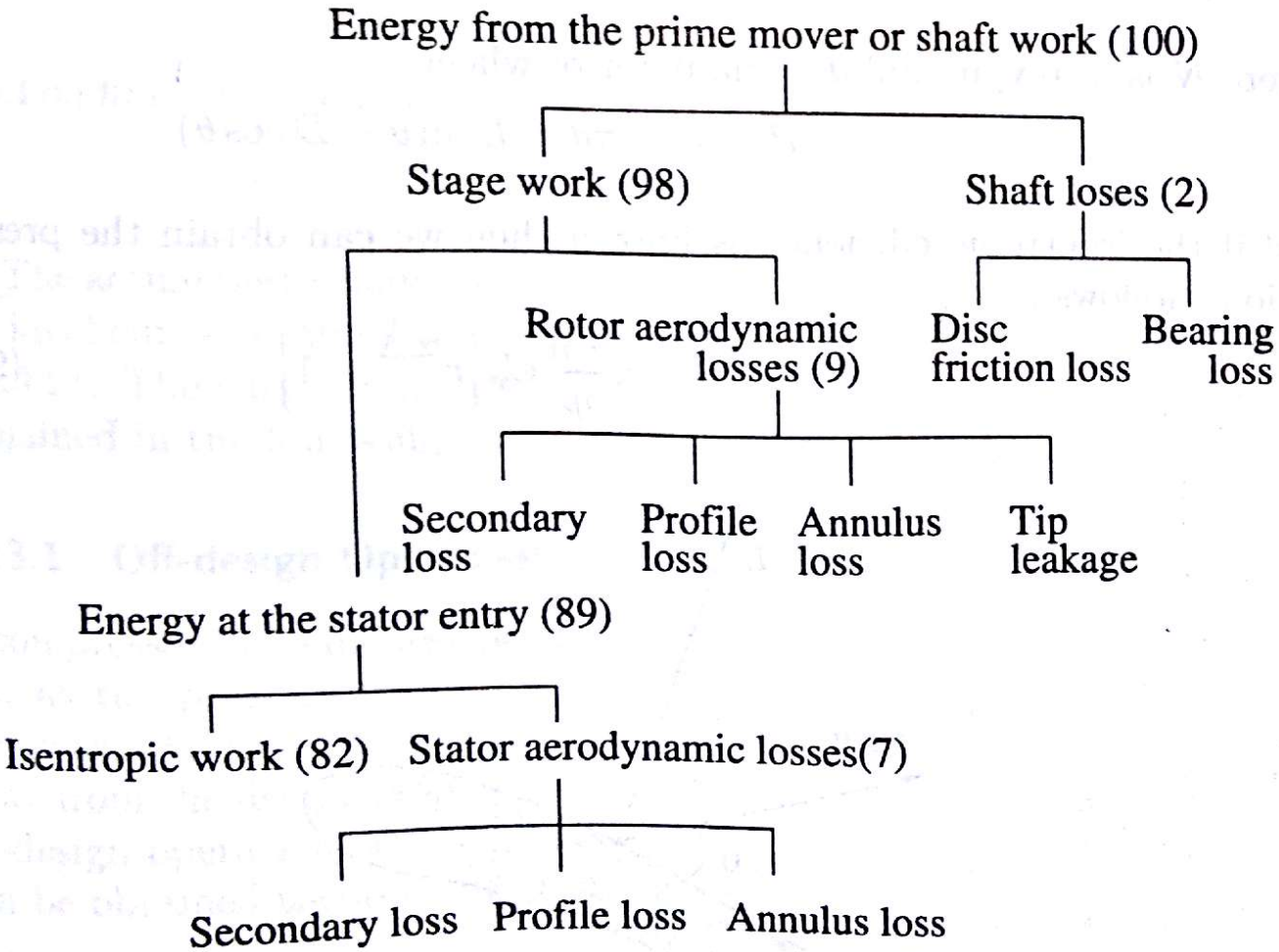

Fig. 9.17 Energy flow diagram for an axial flow compressor stage

an example. The ratio of the isentropic work (82) and the actual stage work (98) gives the stage efficiency, whereas the overall efficiency is directly obtained as 82%.

9.13 PERFORMANCE CHARACTERISTICS

The performance characteristics of axial compressors or their stages at various speeds can be presented in terms of the plots of the following parameters:

(i) Pressure rise vs flow rate,

$$\Delta p = f(Q) = f(m)$$

(ii) Pressure ratio vs non-dimensional flow rate (Fig.9.19),

$$\frac{p_2}{p_1} = f\left(\frac{m\sqrt{T_{01}}}{p_{01}}\right)$$

(iii) Loading coefficient vs flow coefficient (Fig.9.20),

$$\psi = f(\phi) \tag{9.83}$$

The actual performance curve based on measured values is always below the ideal curve obtained theoretically on account of losses. This is shown in Fig.9.21. The surge point and stable and unstable flow regimes have been explained in the following sections.

9.13.1 Off-design Operation

A compressor gives its best performance while operating at its design point, i.e., at the pressure ratio and flow rate for which it has been designed. However, like any other machine or system, it is also expected to operate away from the design point. Therefore, a knowledge about its behaviour at off-design operation is equally important. Off-design characteristic curves can be obtained theoretically from Eq. 9.44.

$$\psi = \phi(\tan\beta_1 - \tan\beta_2) = \phi(\tan\alpha_2 - \tan\alpha_1) \tag{9.84}$$

But,

$$\tan\alpha_2 = \frac{1}{\phi} - \tan\beta_2$$

Therefore,

$$\psi = 1 - \phi(\tan\beta_2 + \tan\alpha_1) \tag{9.85}$$

The quantity $(\tan\beta_2 + \tan\alpha_1)$ can be assumed constant in a wide range of incidence up to the stalling value *is*. This is justified in view of small variations in the air angles at the rotor and stator exits. Therefore, writing $\alpha_1 = \alpha_3$,

$$A = \tan\beta_2 + \tan\alpha_3 \tag{9.86}$$

If the design values are identified by the superscript*, Eq. 9.85 along with Eq. 9.86 can be written as

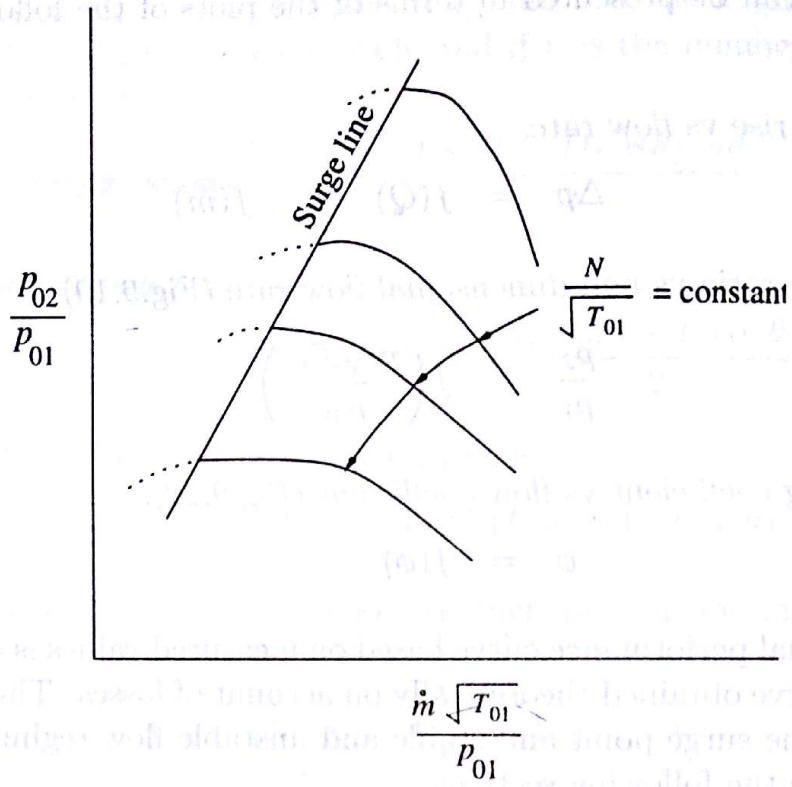

Fig. 9.19 Performance curves of a compressor

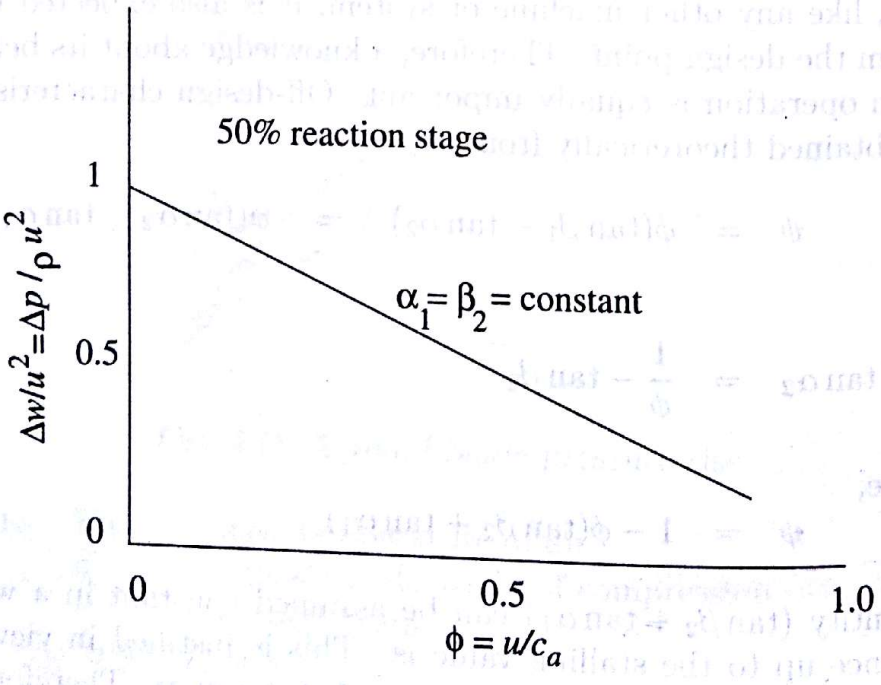

Fig. 9.20 Variation of pressure coefficient with flow coefficient for an axial flow compressor stage

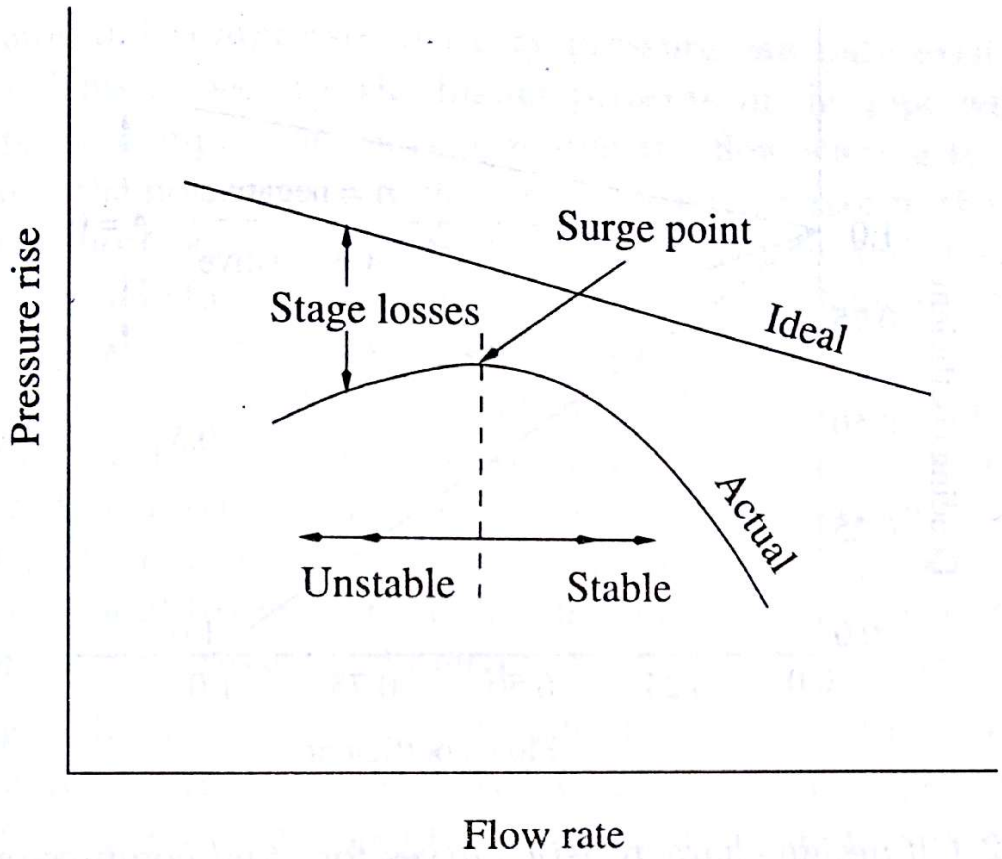

Fig. 9.21 Ideal and actual performance curves for an axialcompressor

$$\psi^* = 1 - A\phi^* \tag{9.87}$$

$$A = \frac{1-\psi^*}{\phi^*}$$

At off-design conditions

$$\psi = 1 - A\phi = 1 - (1-\psi^*)\frac{\phi}{\phi^*} \tag{9.88}$$

This equation also gives the off-design characteristic of an axial flow compressor. Figure 9.22 shows theoretical values of A, the curves are falling while for negative values rising characteristics are obtained. The actual curves will be similarly modified but slightly on account of losses.